Acta Crystallographica Section B
Structural Science
ISSN 0108-7681

Atomic interactions in ethylenebis(1-indenyl)zirconium dichloride as derived by experimental electron density analysis

Adam I. Stash,[a] Kiyoaki Tanaka,[b] Kazunari Shiozawa,[c] Hitoshi Makino[d] and Vladimir G. Tsirelson[e]*

[a]L. Ya. Karpov Institute of Physical Chemistry, Vorontsovo Pole 10, Moscow 103064, Russia, [b]Nagoya Institute of Technology, Gokiso-cho, Showa-ku, Nagoya 466, Japan, [c]Mitsui Chemical Analysis and Consulting Service Inc., Nagaura 580-32, Sodegaura, Chiba 299-0265, Japan, [d]Taiyo Yuden Co. Ltd, Engineering Division-II Ferrite Application Product Unit, 1796-1 Kawai Tamamura-machi, Sawa-gun Gunnma, Japan, and [e]D. I. Mendeleev University of Chemical Technology, Miusskaya sq., 9, Moscow 125047, Russia

Correspondence e-mail: tsirel@muctr.edu.ru

Received 18 February 2005
Accepted 3 May 2005

A topological analysis of the experimental electron density in *racemic* ethylenebis(1-indenyl)zirconium dichloride, $C_{20}H_{16}Cl_2Zr$, measured at 100 (1) K, has been performed. The atomic charges calculated by the numerical integration of the electron density over the zero-flux atomic basins demonstrate the charge transfer of 2.25 e from the Zr atom to the two indenyl ligands (0.19 e to each) and two Cl atoms (0.93 e to each). All the atomic interactions were quantitatively characterized in terms of the electron density and the electronic energy-density features at the bond critical points. The Zr—C2 bond paths significantly curved towards the C1—C2 bond were found; no other bond paths connecting the Zr atom and indenyl ligand were located. At the same time, the π-electrons of the C1—C2 bond are significantly involved in the metal–ligand interaction. The electron density features indicate that the indenyl coordination can be approximately described as η^1 with slippage towards η^2. The 'ligand-opposed' charge concentrations around the Zr atom were revealed using the Laplacian of the electron density and the one-particle potential; they were linked to the orbital representations. Bonds in the indenyl ligand were characterized using the Cioslowski–Mixon bond-order indices calculated directly from the experimental electron density.

1. Introduction

Recently there has been interest in the research of zirconocenes because of their application in polymerization catalysis and organic syntheses (Brintzinger *et al.*, 1995; Kaminsky & Arndt, 1997; Green, 1998; Ivchenko & Nifantiev, 1998). In particular, *ansa*-bridged derivatives of dichlorozirconocene, in which two cyclopentadienyl or indenyl groups are linked together by a bridging group (Nesmeyanov *et al.*, 1956; Rinehart & Curby, 1957), are important in the synthesis of the isotactic polypropylene (Long, 1998; Togni, 1998). An insight into the details of the electron density distribution can clarify the nature of the metal–ligand interactions in these catalysts. In this work we focus on the electron density features in racemic ethylenebis(1-indenyl)zirconium dichloride, $C_{20}H_{16}Cl_2Zr$, (*rac*-EBIZD) – the classic zirconocene (Ewen, 1984; Kaminsky *et al.*, 1985) which is often used as a reference compound in the studies of new metallocenes.

The electronic structure of the metallocenes was qualitatively described in terms of orbital representations many years ago (Lauher & Hoffmann, 1976; Green, 1998). Recently, detailed Hartree–Fock and DFT calculations of the orbital structure of some metallocenes have been performed (Green, 1998; Linnolahti *et al.*, 2001; Frenking *et al.*, 2003; Zachmanoglu *et al.*, 2002; Xu *et al.*, 2003; Belelli *et al.*, 2004; Tamm *et*

Table 1
Crystallographic data and selected experimental information for *rac*-EBIZD.

Crystal data	
Chemical formula	$C_{20}H_{16}Cl_2Zr$
M_r	418.45
Cell setting, space group	Monoclinic, *C*2/*c*
a, *b*, *c* (Å)	15.3870 (5), 10.5120 (5), 11.9270 (5)
β (°)	121.85 (1)
V (Å^3)	1638.7 (2)
Z	4
D_x (Mg m^{-3})	1.696
Radiation type	Mo $K\alpha$
No. of reflections for cell parameters	40
θ range (°)	30.0–35.0
μ (mm^{-1})	0.99
Temperature (K)	100 (2)
Crystal form, colour	Sphere, colourless
Crystal radius (mm)	0.09 (1)
Data collection	
Diffractometer	MacScience four-circle
Data collection method	$\omega/2\theta$
Absorption correction	For a sphere
T_{min}	0.861
T_{max}	0.863
No. of measured, independent and observed reflections	10 224, 6602, 6151
Criterion for observed reflections	$I > 2\sigma(I)$
R_{int}	0.020
θ_{max} (°)	50.0
Range of *h*, *k*, *l*	$-33 \Rightarrow h \Rightarrow 28$ $-22 \Rightarrow k \Rightarrow 18$ $-19 \Rightarrow l \Rightarrow 25$
No. and frequency of standard reflections	3 every 30 reflections
Intensity decay (%)	1.5
Refinement	
Refinement on	F^2
$R[F^2 > 2\sigma(F^2)]$, $wR(F^2)$, S	0.030, 0.072, 1.02
No. of reflections	6602
No. of parameters	137
H-atom treatment	Refined independently
Weighting scheme	$w = 1/[\sigma^2(F_o^2) + (0.0356P)^2 + 1.3284P]$, where $P = (F_o^2 + 2F_c^2)/3$
$(\Delta/\sigma)_{max}$	0.002
$\Delta\rho_{max}$, $\Delta\rho_{min}$ (e Å^{-3})	1.37, −1.44

Computer programs used: *SHELXS*97 (Sheldrick, 1997*a*), *SHELXL*97 (Sheldrick, 1997*b*).

al., 2004). At the same time, only few experimental and theoretical studies of metallocenes deal with the electron density distribution. The X-ray experimental deformation electron density has been analyzed in (η^5-C_5H_5)Fe[η^5-$PC_4H_2(CH_3)_2$] (Weits *et al.*, 1981), (η^5-C_5H_5)$_2$V (Antipin *et al.*, 1996; Lyssenko *et al.*, 2001) and (η^5-C_5H_5)Ti(η^8-C_8H_8), and (η^5-C_5H_5)M(η^5-C_7H_7) with M = Ti, V, Cr (Lyssenko *et al.*, 2001). Topological features of the experimental electron density in the imine coupling product with open zirconocene were elucidated by Pillet *et al.* (2003) and Coppens *et al.* (2005). Theoretical electron densities of metallocenes M(η^5-C_5H_5)$_2$ (M = Mg, Ca; Bytheway *et al.*, 1996), M(C_5H_5)$_2$ (M = V, Cr, Mn, Fe, Co, Ni; Lyssenko *et al.*, 2003), Cp_2ZrCl_2/methylaluminoxane (Belelli *et al.*, 2004), group 5 bent metallocene complexes (Fan & Lin, 1998), and a model complex, which represents interaction of Ti atom with the cyclopentadienyl and cyclohexadienyl ligands (Bader & Matta, 2001), were also studied in a topological analysis.

Topological electron-density analysis (Bader, 1990) has proved to be an appropriate tool for studying a wide spectrum of metal–ligand interactions. The main achievements in this area are summarized by Popelier *et al.* (2000), Koritsanszky & Coppens (2001), Tafipolsky *et al.* (2002), Macchi & Sironi (2003) and Scherer & McGrady (2004). Knowledge of the electron density, $\rho(\mathbf{r})$, the gradient field of the electron density, $\nabla\rho(\mathbf{r})$, the Laplacian of the electron density, $\nabla^2\rho(\mathbf{r})$, the local electronic energy, $h_e(\mathbf{r})$, as well as the kinetic energy density, $g(\mathbf{r}) > 0$, and potential energy density, $v(\mathbf{r}) < 0$ [$h_e(\mathbf{r}) = g(\mathbf{r}) + v(\mathbf{r})$], allows a network of atomic interaction lines to be established, *i.e.* the molecular graph, and allows each atomic interaction type to be determined and quantified. Consideration of these functions at the bond critical points allows one to distinguish between closed-shell atomic interactions ($\rho_b <$ 0.3 e Å^{-3}, $\nabla^2\rho_b > 0$, $|\lambda_1|/\lambda_3 < 0.25$,[1] $h_{e,b} > 0$, $|v_b|/g_b < 1$ and g_b/ρ_b > 1), shared interactions ($\rho_b > 1.0$ e Å^{-3}, $\nabla^2\rho_b < 0$, $|\lambda_1|/\lambda_3 > 1$, $h_{e,b} < 0$, $|v_b|/g_b > 2$ and $g_b/\rho_b < 1$) and intermediate interactions ($0.3 < \rho_b < 1.0$ e Å^{-3}, $\nabla^2\rho_b > 0$, $|\lambda_1|/\lambda_3 > 0.20$, $h_{e,b} < 0$, and $1 < |v_b|/g_b < 2$ and $g_b/\rho_b > 1$; Macchi *et al.*, 1998; Tsirelson, 1999; Bianchi *et al.*, 2000; Espinosa *et al.*, 2002; Macchi & Sironi, 2003; Marabello *et al.*, 2004). It is important that such a quantitative description of bonding can be directly performed using the experimental electron density (Abramov, 1997; Espinosa *et al.*, 1998; Tsirelson, 2002, 2003), provided that $g(\mathbf{r})$ is approximated using the formulae of the density-functional theory (Parr & Yang, 1989) as those derived by Kirzhnits (1957) or Lee *et al.* (1991). The potential energy density, $v(\mathbf{r})$, can then be calculated according to Espinosa *et al.* (1998) using a local form of the virial theorem (Bader & Beddall, 1972). For closed-shell and intermediate atomic interactions, this approximation leads to values of $g(\mathbf{r})$, $v(\mathbf{r})$ and $h_e(\mathbf{r})$, which are in good agreement with values derived by the Hartree–Fock or Kohn–Sham methods (Farrugia *et al.*, 2003; Tsirelson, 2003). For shared interactions, the approximate values of $g(\mathbf{r})$, $v(\mathbf{r})$ and $h_e(\mathbf{r})$ near the centers of internuclear distances are distorted due to the large negative values of the Laplacian term, which is used in the formulae mentioned above to correctly describe the local behaviour of $g(\mathbf{r})$. Thus, the energy-density consideration is generally restricted to the closed-shell and intermediate atomic interactions if analysis is based on the experimental electron density.

We applied the topological analysis to the experimental electron density of *rac*-EBIZD considering the whole space distribution of the electron density, the Laplacian of the electron density and the local electronic energies, and the critical point features. The deformation and valence electron densities, and a one-particle potential (Hunter, 1975; Tsirelson & Stash, 2004) were also derived. To our knowledge, this work is the first study of experimental electron density in a metal complex with indenyl ligands.

[1] λ_1 is the most negative electron-density curvature in the direction perpendicular to the internuclear line, while $\lambda_3 > 0$ is the electron-density curvature along this line.

Table 2
Topological electron-density characteristics at the bond critical points in *rac*-EBIZD.

$\rho(\mathbf{r}_b)$ is the electron density, $\nabla^2\rho(\mathbf{r}_b)$ is the Laplacian of the electron density, $\varepsilon = |\lambda_1/\lambda_2| - 1$ is the ellipticity of the electron density at the bond critical point (Bader, 1990), where $\lambda_1 < \lambda_2$ are the negative electron-density curvatures in the directions perpendicular to the internuclear line.

Bonds	Internuclear distances (Å)	$\rho(\mathbf{r}_b)$ (e Å^{-3})	$\nabla^2\rho(\mathbf{r}_b)$ (e Å^{-5})	ε
Zr—Cl	2.424 (1)	0.41 (2)	6.06 (10)	0.182
Zr—C2	2.465 (1)	0.32 (2)	3.90 (8)	1.718
C1—C2	1.424 (2)	2.12 (1)	−18.23 (8)	0.548
C1—C71	1.422 (1)	1.96 (1)	−16.64 (8)	0.414
C1—C8	1.504 (1)	1.80 (1)	−12.01 (8)	0.103
C2—C3	1.421 (2)	2.13 (1)	−19.07 (8)	0.233
C3—C31	1.421 (2)	2.04 (1)	−16.61 (8)	0.347
C31—C4	1.425 (1)	2.09 (1)	−17.03 (8)	0.232
C31—C71	1.440 (1)	1.95 (1)	−13.36 (8)	0.272
C4—C5	1.369 (2)	2.31 (1)	−22.29 (8)	0.210
C5—C6	1.428 (2)	2.11 (1)	−16.97 (8)	0.207
C6—C7	1.370 (2)	2.30 (1)	−21.91 (8)	0.204
C7—C71	1.429 (1)	2.08 (1)	−17.13 (8)	0.104
C8—C8′	1.535 (2)	1.70 (1)	−8.50 (8)	0.363
C2—H2†	1.083	1.86 (1)	−20.85 (6)	0.085
C3—H3	1.083	1.87 (1)	−21.19 (6)	0.089
C4—H4	1.083	1.85 (1)	−18.84 (6)	0.039
C5—H5	1.083	1.85 (1)	−18.99 (6)	0.040
C6—H6	1.083	1.85 (1)	−18.84 (6)	0.040
C7—H7	1.083	1.84 (1)	−18.65 (6)	0.036
C8—H81	1.092	1.68 (1)	−12.23 (6)	0.119
C8—H82	1.092	1.88 (1)	−17.30 (6)	0.127

† The C—H bond lengths were fixed at the standard values – see text.

2. Experimental

rac-EBIZD has been prepared according to Piemontesi *et al.* (1995). Single crystals appeared after the mixture was kept in tetrahydrofuran solution for 12 h. After filtration, the crystals were dried under vacuum. A spherical sample with r = 0.09 (1) mm was prepared. The measurements were taken at 100 (1) K on a Mac Science four-circle automatic diffractometer with a molybdenum rotating-anode X-ray source (50 kV, 90 mA) in the scan mode $\omega/2\theta$ with a scan speed of 2° min^{-1}. A scan range of 1.2 + 0.5tan θ was applied. The stability of the intensities was controlled by measuring the $\bar{2}00$, $0\bar{2}0$ and $\bar{4}02$ reflections every 30 reflections. Multiple diffraction was avoided by using the ψ-scan method (Tanaka & Saito, 1975). The greatest variations in intensity were less than 1.5% during the experiment. The unit-cell parameters (space group $C2/c$) were determined with 40 reflections from the $30 < \theta < 35°$ scattering angle range.

There were 10 224 diffraction intensities with indices in the range $-33 < h < 28$, $-22 < k < 18$, $-19 < l < 25$ recorded; the statistical intensity precision of 1–2% has been reached. After the background subtraction, intensities were corrected for the Lorentz and polarization factors, and absorption (μr = 0.09). Merging of the intensities yielded 6612 independent intensities, R(int) = 0.02; 5239 independent intensities with $I > 3\sigma(I)$ were used in further analysis. Crystallographic data and the experimental details for the *rac*-EBIZD crystal are listed in Table 1.

3. Refinement

3.1. Spherical-atom refinement

The structure of *rac*-EBIZD was refined by full-matrix least-squares using the spherical-atom model. The atomic relativistic scattering factors and anomalous scattering corrections were taken from the *International Tables for Crystallography* (1995). Atomic coordinates from Piemontesi *et al.* (1995) were used as the initial approximation in the refinement. The atomic displacements were modeled in the anisotropic harmonic approximation. An attempt to account for the isotropic secondary extinction according to Becker & Coppens (1974) showed that this effect was negligible in the sample under examination [$I_{corr} = yI_{obs}$, y = 1.00 (1)].

3.2. Multipole refinement

The multipole structural model of Hansen & Coppens (1978) has been used in a subsequent refinement. The atomic 'many-configuration' relativistic wavefunctions of Macchi & Coppens (2001) were used to describe both the core- and the valence-electron shells. Anomalous dispersion corrections were taken from *International Tables for Crystallography* (1995). Atomic displacements were described in the anisotropic harmonic approximation as before.

Refinement based on $|F|$ with least-squares weights of $1/[\sigma^2(F) + 0.0005F^2]$ was carried out using *MOLDOS*2004 (Stash, 2003), a modified version of the programs *MOLDOS*97 (Protas, 1995) and *MOLLY* (Hansen & Coppens, 1978). Firstly, the positional parameters and atomic displacement parameters of the non-H atoms were refined in the high-angle region ($\sin\theta/\lambda > 0.70$ Å^{-1}), while the hydrogen displacement parameters were determined using low-angle ($\sin\theta/\lambda < 0.7$ Å^{-1}) reflections. The C—H bond distances were elongated up to the standard recommended values of 1.083 Å for C—H bonds and 1.092 Å for C—H$_2$ bonds (*International Tables for Crystallography*, 1995) to provide a more accurate representation of the C—H bonds. Secondly, scale factors and multipole parameters for all the atoms were refined in the range $0.0 < \sin\theta/\lambda < 1.08$ Å^{-1}. The initial electronic configuration of the Zr atom was taken to be [Kr]$4d^2 5s^2$. Only one set of multipole parameters was refined for the chemically equivalent carbon (C1, C2 ↔ C3, C4 ↔ C5 ↔ C6 ↔ C7, C31 ↔ C71, C8) and hydrogen (H2 ↔ H3, H4 ↔ H5 ↔ H6 ↔ H7, H81 ↔ H82) atoms. The contraction/expansion parameters κ for the H atoms were taken as 1.2 and were not varied. The refinement of the model described was stable; it was successively repeated until convergence was achieved. An attempt to change the electronic configuration of the Zr atom to an ionic one destroyed the stability of the refinement.[2] The refinement indices are R = 0.026, wR = 0.037, S = 1.21.

The model total electron density in *rac*-EBIZD, reconstructed using the multipole parameters obtained, appeared to

[2] Supplementary data for this paper, including atomic charges based on the multipole model, κ values as well as the atomic positions and equivalent atomic displacement parameters, are available from the IUCr electronic archives (Reference: BS5015). Services for accessing these data are described at the back of the journal.

be positive everywhere. The residual maps (which have been deposited) showed peaks at 0.5 e Å^{-3} close to the Zr position, and a flat distribution of *ca* ± 0.1 e Å^{-3} on the Zr—C2 and Zr—C1 lines and in the plane of the indenyl rings.

Calculated characteristics of the bond critical points in the electron density are listed in Table 2. The network of bond paths (Fig. 1*b*) and maps of the deformation and valence electron density, and one-electron potentials in selected planes are shown in Figs. 2–6. All the calculations were performed with a modified version of the *WinXPRO* program (Stash & Tsirelson, 2002, 2005).

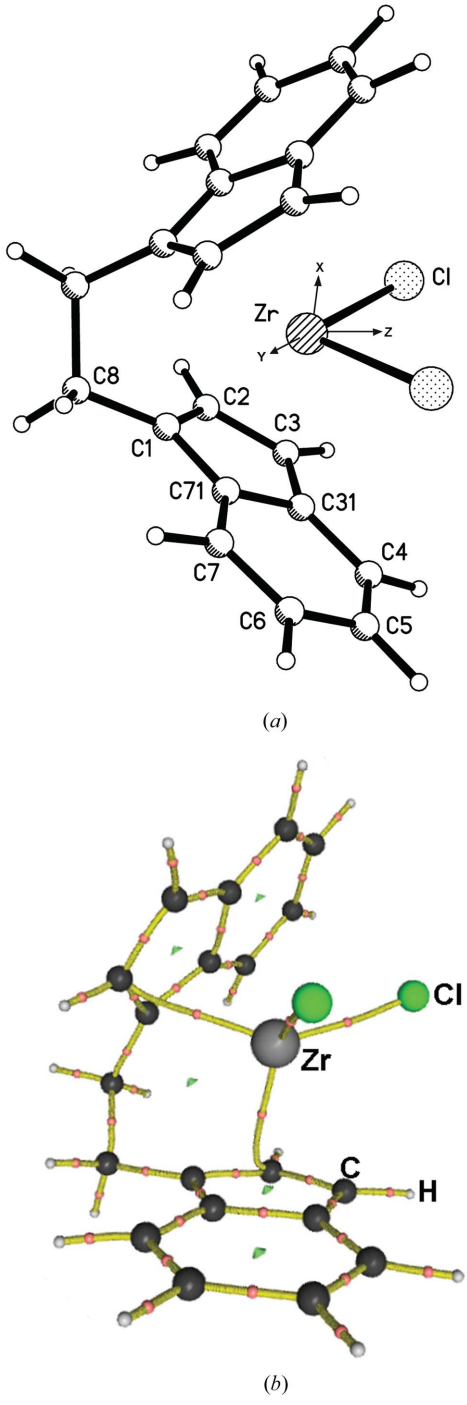

Figure 1
(*a*) Geometry, atomic numbering and (*b*) the bond path network in *rac*-EBIZD. The bond critical points are shown as red circles, while the ring critical points are depicted as green triangles.

4. Results and discussion

4.1. Molecular structure

The crystal and molecular structure of *rac*-EBIZD has been described by Wild *et al.* (1985), Schaefer *et al.* (1987) and Piemontesi *et al.* (1995). The molecule has crystallographically imposed C_2 symmetry; its structure (Fig. 1*a*) is characterized by an angle between the least-squares ring planes of 60.4° and a torsional angle (C1—C8—C8′—C1′) of 47.6°. A small deviation from planarity of the indenyl fragment has been found: the mean deviation from the least-squares plane through all independent C atoms is 0.026 Å. Angles Cl—Zr—Cl, C2—Zr—C2 and Cl—Zr—C2 are 96.9 (1), 107.4 (1) and 94.9 (1)°, respectively. The internuclear distance *R*(Zr—C2) of 2.465 (1) Å is the shortest of the metal–indenyl ligand distances in *rac*-EBIZD; other distances are *R*(Zr—C1) = 2.492 (1), *R*(Zr—C3) = 2.534 (1), *R*(Zr—Cl) = 2.424 (1) Å.

4.2. Atomic charges

The atomic charges calculated by the numerical integration of the electron density over zero-flux atomic basins Ω_i (Bader, 1990) are listed in Table 3. They show a transfer of 2.25 e from the Zr atom to both indenyl ligands and two Cl atoms: 0.93 e are associated with each Cl atom, while 0.19 e are transferred to each indenyl ligand. Pillet *et al.* (2003) have reported a charge transfer of 2.16 e from the Zr atom to ligands in a similar complex – an imine coupling product with zirconocene – which is similar to our result.

The C_2H_4 bridge carries a positive net charge of 0.08 e. This quantity is too small to make any conclusion about the donor–acceptor properties of the bridge fragment.

4.3. Features of the electron density and Zr-ligand bond paths

We have found all the critical points in the electron density, the type and number of which obey the Poincare–Hopf–Morse condition (Zou & Bader, 1994; Martin Pendas *et al.*, 1997). The critical points are shown in Fig. 1(*b*) together with the network of bond paths defining the molecular graph of *rac*-EBIZD. Characteristics of the bond critical points and corresponding internuclear distances are listed in Table 2. A fragment of the three-dimensional representation of the electron density illustrating the coordination of the Zr atom by the indenyl ligands has been deposited. Only one Zr—C2 bond path exists between the metal and each indenyl ligand (the distance from Zr to the corresponding bond critical point is 1.252 Å). This bond path is significantly curved towards the C1—C2 bond and its length of 2.587 Å is noticeably different from the internuclear vector length (see Table 3). The distance of the corresponding bond critical-point position from the internuclear vector is 0.194 Å; such a deviation does not exceed 0.06 Å for other bonds.

Table 3
Atomic charges from the numerical integration within zero-flux atomic basins in the asymmetric unit.

Atom	Atomic charge (e)	Atom	Atomic charge (e)
Zr	+2.25	C71	−0.21
Cl	−0.93	C8	0.14
C1	−0.17	H2	0.28
C2	−0.20	H3	0.27
C3	−0.21	H4	0.17
C31	−0.12	H5	0.18
C4	−0.14	H6	0.18
C5	−0.14	H7	0.18
C6	−0.13	H81	−0.03
C7	−0.17	H82	−0.07

The total calculated charge of the molecule is +0.02 e, which represents the global error due to the numerical integration procedure.

Checking a three-dimensional field of the electron-density gradient did not reveal any evidence of a Zr—C2 bond path bifurcation, a branch of which goes to the C—C bond. Thus, according to the topological analysis, the Zr atom is directly bonded to the C2 atom of the indenyl ligands only. Figs. 2–4 help us to understand the nature of this bonding feature. Every Zr—C2 bond path travels through the maximum in the negative Laplacian of the electron density, which is located near the C2 atom (Fig. 2). These maxima, lying on the line connecting the C2 atoms of the neighbouring ligands, correspond to the charge concentrations in the valence shells of the C2 atoms. No other out-of-plane charge concentrations near the C atoms in the indenyl ligands were found (Figs. 4 and 6). This finding is in line with earlier observations dealing with the metal–ligand interactions in different metallocenes (Bytheway *et al.*, 1996; Bader & Matta, 2001; Pillet *et al.*, 2003). The location of the charge concentrations mentioned earlier, the anomalously large electron-density anisotropy in the planes perpendicular to the Zr—C2 direction as well as the significant ellipticity of the C1—C2 bond (see Table 2 and Fig. 3) prove that π-electrons of the C1—C2 bond are involved in the metal–ligand interaction.

Thus, the whole set of electron density features that characterize the metal–indenyl bonding in *rac*-EBIZD, including the Zr—C2 bond path, point to the conclusion that the indenyl coordination can be approximately described as η^1 with slippage towards η^2.

The quantitative electron-density and energy-density characteristics of the bond critical point corresponding to the Zr—C2 interaction (Tables 2 and 4) satisfy the following conditions: $\rho(\mathbf{r}_b) < 0.5$ e Å^{-3}, $\nabla^2\rho(\mathbf{r}_b) > 0$ as found for closed-shell interactions; $h(\mathbf{r}_{e,b}) < 0$ as found for shared interactions. $|v(\mathbf{r}_b)|$ only slightly exceeds $g(\mathbf{r}_b)$: $|v(\mathbf{r}_b)|/g(\mathbf{r}_b) = 1.09$ (the latter reflects the polar character of this interaction). In addition, $g(\mathbf{r}_b)/\rho(\mathbf{r}_b) = 0.949$ (shared interaction) and $\lambda_1/\lambda_3 = 0.19$ (polar closed-shell interaction). According to the suggested classification (Bader, 1990; Macchi, 1998; Tsirelson, 1999; Bianchi *et al.*, 2000; Espinosa *et al.*, 2002; Macchi & Sironi, 2003; Marabello *et al.*, 2004), this set of characteristics assigns the Zr—C2 bond to a intermediate polar atomic interaction. It is worth noting that the values of $\rho(\mathbf{r}_b)$ and $\nabla^2\rho(\mathbf{r}_b)$ for the Zr—C2 interaction in *rac*-EBIZD appeared to be very close to the same characteristics of the Zr—C bond of comparable length [2.471 Å; $\rho(\mathbf{r}_b) = 0.31$ e Å^{-3}, $\nabla^2\rho(\mathbf{r}_b) = 3.5$ e Å^{-3}] in an imine coupling product with open zirconocene (Pillet *et al.*, 2003).

The characteristics of the Zr—Cl bond critical point listed in Tables 2 and 4 indicate that this interaction is of nearly pure closed-shell type. However, because of the geometry of the $ZrCl_2$ fragment, this interaction differs from an ionic bond. Deformation and valence electron densities (Fig. 4) show that the lobes of the electron concentration on the p_π orbitals of the Cl atom, which are visibly elongated in the Cl—Zr—Cl plane, are involved in an interaction with the *d*-orbital of the Zr atom directed along the bisector of the Cl—Zr—Cl angle (see Fig. 4*e*). That is in agreement with Lauher & Hoffmann's

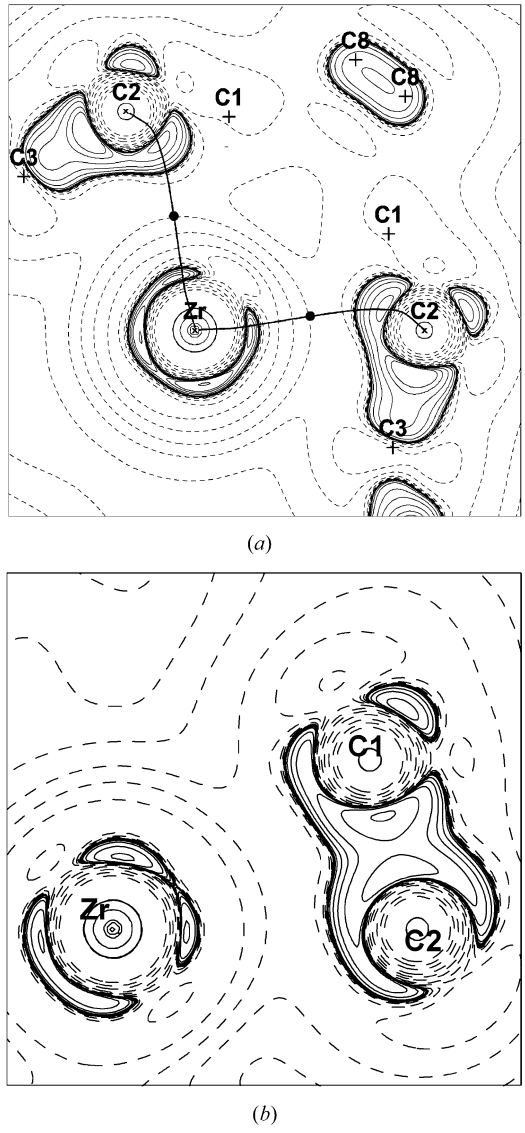

Figure 2
Laplacian of electron density in (*a*) the C2—Zr—C2 plane and (*b*) the C1—Zr—C2 plane of *rac*-EBIZD overlaid with the Zr—C2 bond paths. Bond critical points are depicted as black points. Line intervals are $\pm$ (2, 4, 8) $\times 10^n$ e Å^{-5} ($-3 \le n \le 3$), negative values are solid. The projections of the out-of-plane C1, C3 and C8 atoms are shown as crosses.

Table 4
Electronic energy characteristics of the metal–ligand interactions at the bond critical points in *rac*-EBIZD.

$\rho(\mathbf{r}_b)$ is the electron density, $\nabla^2\rho(\mathbf{r}_b)$ is the Laplacian of the electron density, $g(\mathbf{r}_b)$, $v(\mathbf{r}_b)$, $h(\mathbf{r}_b)$ are kinetic, potential and electronic energy densities, respectively.

Bonds	$g(\mathbf{r}_b)$ (a.u.)	$g(\mathbf{r}_b)/\rho(\mathbf{r}_b)$	$v(\mathbf{r}_b)$ (a.u.)	$\lvert v(\mathbf{r}_b)\rvert/g(\mathbf{r}_b)$	$h(\mathbf{r}_b)$ (a.u.)	$h(\mathbf{r}_b)/\rho(\mathbf{r}_b)$
Zr—Cl	0.069	1.125	−0.076	1.10	−0.007	−0.114
Zr—C2	0.045	0.949	−0.049	1.09	−0.004	−0.084

(1976) statement that the ligand π-orbital eclipses the a_1 orbital of the metal in the bent d^0 metallocenes.

The Zr—C2 and Zr—Cl interactions differ in the bond degree parameter $h(\mathbf{r}_b)/\rho(r_b)$ (Table 4). Following Espinosa *et al.* (2002), we conclude that the Zr—Cl interaction is stronger.

We have to point out that the bond-type attribution used above is based only on the bond critical-point properties. It is rather restricted in some aspects. First, the differentiation of atomic interactions within the same interaction type is vague. Second, the Laplacian of the electron density does not resolve the outermost and penultimate shells of the 4*d* metals (Sagar *et al.*, 1988; Shi & Boyd, 1988; Bader, 1990; Schmider *et al.*, 1991; Kohout *et al.*, 1991; Tsirelson & Ozerov, 1996), making the attribution of the interactions involving such atoms difficult. For example, the Laplacian of a free Zr atom exhibits only four pairs of minima and maxima, whereas five electronic shells exist in this atom. In addition, the Zr—C2 bond critical point is placed in a region of relatively flat interatomic electron density, which is far from the Laplacian nodal surface. In this respect, the Zr—C2 interaction differs from the image of intermediate interactions in molecules, which consist of the main group atoms (Bader, 1990). Similar observations for the metal–ligand bonds in the coordination compounds based on the experimental Laplacian were also reported by Smith *et al.* (1997), Wang *et al.* (1997), Hwang & Wang (1998), Lee *et al.* (1999) and Macchi & Sironi (2003).

4.4. Electron density around Zr

Distributions of the Laplacian of the electron density around the Zr atom in *rac*-EBIZD are presented in Figs. 2 and 5. The outer charge concentration area has the 'horseshoe' form, which spans the Zr atom core (Fig. 2). This area shows four $-\nabla^2\rho$ maxima, which are *ca* 0.6 Å from the Zr position and form a distorted tetrahedron. Two Laplacian negative maxima of −46.5 e Å^{-5} are opposed to the Cl atoms; the other two of −42.5 e Å^{-5} are opposed to the C2 atoms and are immersed in the area of negative Laplacian values, which is extended perpendicular to the Cl—Zr—Cl plane.

Bythway *et al.* (1995), Gillespie *et al.* (1996), Bader *et al.* (1998) and Gillespie *et al.* (2004) have noted that the maxima of the negative Laplacian of the electron density around the heavy atoms appear in non-centrosymmetric molecules as 'ligand-opposed' charge concentrations. The Laplacian picture described above is in accordance with these observations. At the same time, elucidation of the nature of the Laplacian features around Zr in *rac*-EBIZD requires further comment.

In the multipole model, the density contributions from both core and valence orbitals are presented in the form of spherical and non-spherical atomic components. As previously mentioned, the different orbital contributions to the non-sphericity of the outer electron shells of the Zr atom are not distinguished by the Laplacian due to the Laplacian properties of heavy atoms. Bader *et al.* (1998) and Gillespie *et al.* (2004) have stressed the difference in the core-valence partition of the electron density resulting from the specific partition scheme applied. Each atomic electronic shell is defined in terms of the orbital representations as the set of occupied

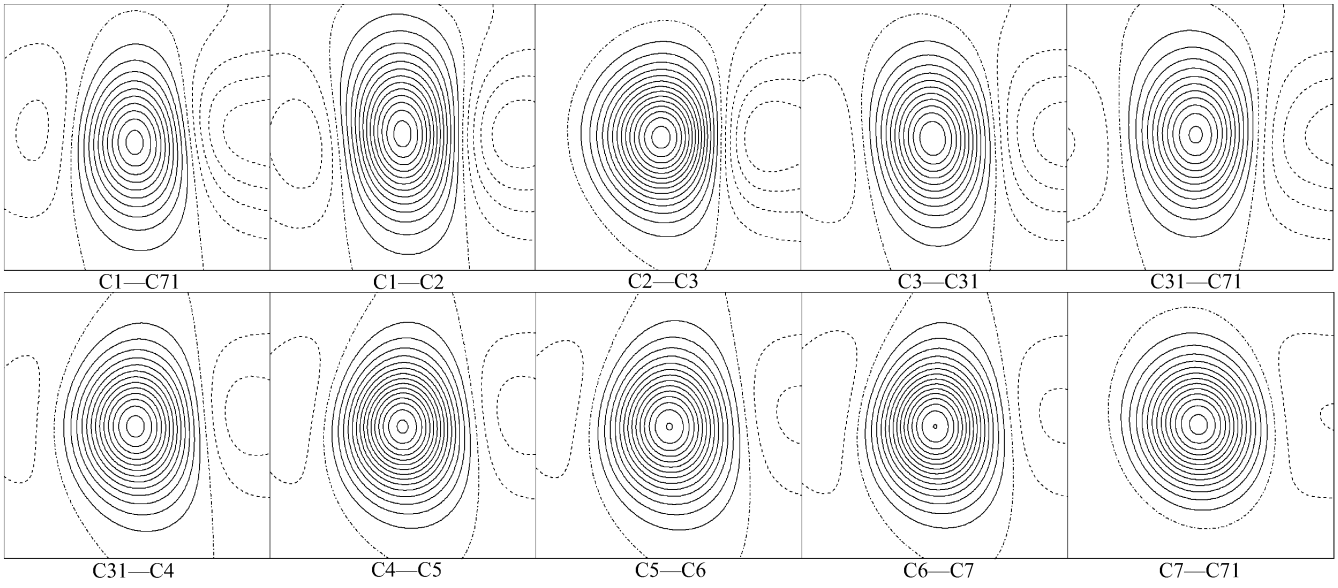

Figure 3
Deformation electron density in the planes which are perpendicular to the C—C bonds of indenyl at the bond critical points. The vertical direction is perpendicular to the ring plane. The line interval is 0.1 e Å^{-3}; the excessive density values are solid.

atomic orbitals with a given principal quantum number. On the other side, the Laplacian of the total electron density yields a position space representation of atoms in the form of alternating negative minima and positive maxima, pairs of which correspond to the electronic shells. All of the orbitals contribute to each electron-density shell, but specific contributions depend on the number and position of the orbital nodes defining the minima and maxima in the Laplacian of the orbital electron density. Thus, the valence shell is defined by the maximal principal quantum number in *the orbital representation* and by the spatial electron density location within the outermost region in *the Laplacian picture*.

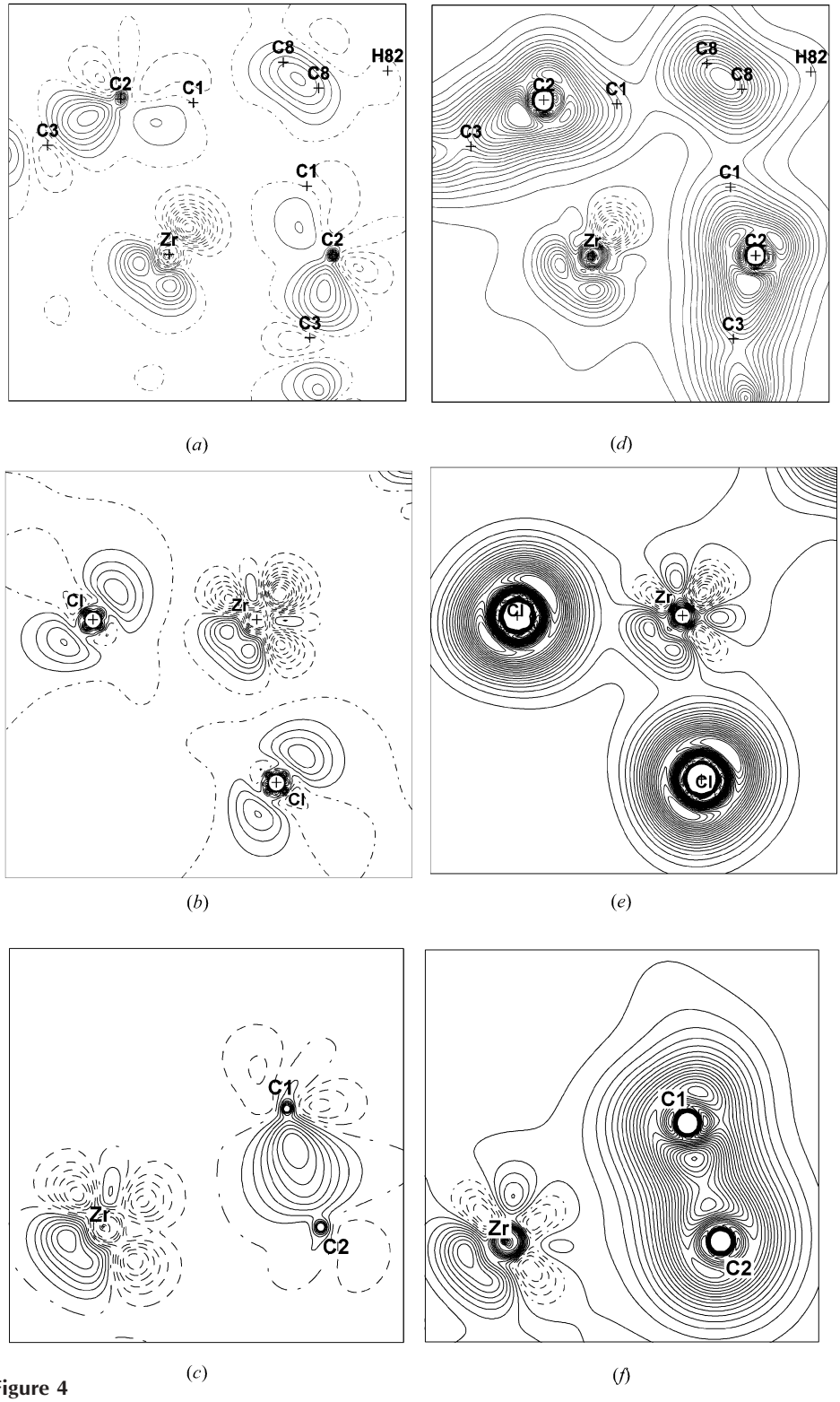

Figure 4
(*a*)–(*c*) Deformation and (*d*)–(*f*) valence electron densities around the Zr atom. The line interval is 0.1 e Å^{-3}; the excessive density values are solid. The projections of the out-of-plane C1, C3, C8 and H82 atoms are shown as crosses.

To clarify a relation between *orbital* and *density-based* descriptions of the electronic shells in the Zr atom, we have calculated the Laplacian of the core electron density (superposition of all the spherical atomic core contributions) and the Laplacian of the valence (non-spherical) part of electron density. The outer fourth $-\nabla^2\rho_{\mathrm{Zr,[Kr]\,core}}$ maximum has a spherical shape and is located 0.61 Å away from the nuclear position. It is close to the *local* maximum positions of ~ 0.60 Å in the negative Laplacian of the total electron density (Fig. 2 and Fig. 5*a*). The outer (fourth) maxima in $-\nabla^2\rho_{\mathrm{Zr,\,valence}}$ are at a distance of 0.45 Å. The fact that the penultimate (fourth) maximum in the negative Laplacian of the electron density of the single 5*s* orbital of Zr is sited 0.43 Å from the nucleus is taken into account, while the outer maximum of $-\nabla^2\rho_{4d}$ is located at the same distance. Therefore, we can conclude that the observed $-\nabla^2\rho$ maxima around the Zr atom (Fig. 2 and Fig. 5*a*) are mainly formed by the density of the 5*s* and 4*d* orbitals, which are partially located in the spatial region associated with the outer core, as defined in terms of the Laplacian of the electron density. Bader *et al.* (1998), Bader & Matta (2001) and Gillespie *et al.* (2004) came to a similar conclusion for molecules containing 3*d* metal atoms.

In contrast to the Laplacian, the one-particle potential (Hunter, 1975; Tsirelson & Stash, 2004) does successfully resolve the

Table 5
4*d*-orbital electron populations for the Zr atom re-calculated from the multipole parameters (the contribution of 5*s* electrons was not explicitly included).

4*d*-orbital populations	Mixing terms
P_{z^2} = 0.41 e	$P_{z^2/xy}$ = 0.11 e
P_{xz} = 0.79 e	P_{z^2/x^2-y^2} = −0.31 e
P_{yz} = 0.75 e	$P_{x^2-y^2/xy}$ = −0.07 e
$P_{x^2-y^2}$ = 0.50 e	$P_{xz/xz}$ = 0.02 e
P_{xy} = 0.22 e	
Total = 2.67 e	Total = −0.25 e

outermost and penultimate shells of the 4*d* metals. The distribution of this function around the Zr atom (Fig. 5*b*) confirms the presence of the 'ligand-opposed' charge concentration described above in terms of the Laplacian of the electron density. We have also calculated the electron localization function (Becke & Edgecombe, 1990; Tsirelson & Stash, 2002*a*) and the localized-orbital locator (Schmider & Becke, 2000; Tsirelson & Stash, 2002*b*) and found the same

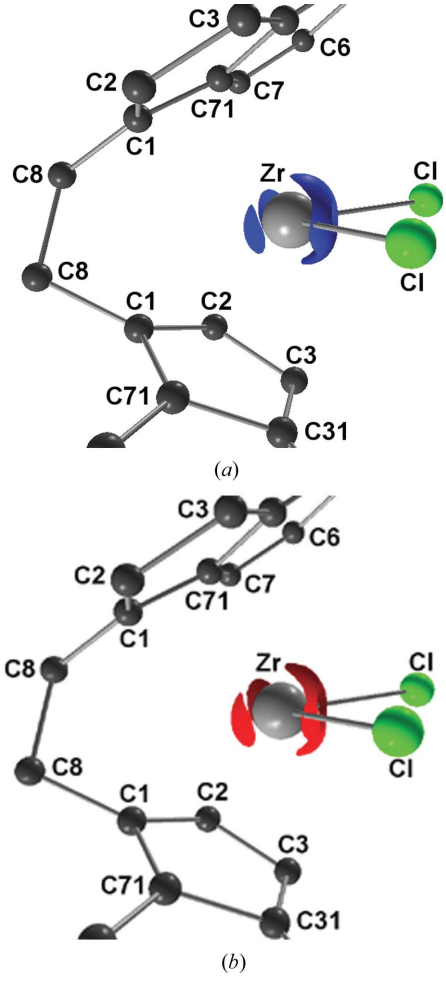

Figure 5
Envelope maps of (*a*) the Laplacian ($\nabla^2\rho = -25$ e Å^{-5}) and (*b*) the one-particle potential ($P = -1.05$ e Å^{-2}), showing the electron density concentrations around the Zr atom. Only the C atoms in the indenyl ligands are depicted.

'ligand-opposed' charge concentrations (these maps are not presented). Thus, the aforementioned charge concentrations are not artifacts and reflect the actual spatial electron arrangement around the Zr atom in *rac*-EBIZD.

Let us turn now to the deformation and valence densities given in Fig. 4 and direct the *z* axis of the local coordinate system on the Zr atom along a bisector of the Cl—Zr—Cl angle, which coincides with the crystallographic twofold rotation axis. The *x* axis is directed towards the ligand (see Fig. 1*a*). A significant distortion of the Zr polyhedron leads to a complicated molecular orbital (MO) picture; however, according to Lauher & Hoffmann (1976) and Green (1998), the main features of bonding in bent metallocenes can be understood with three frontier molecular orbitals, $1a_1$, b_2 and $2a_1$, with metal atomic orbitals (AOs) as the main contributors. The a_1 MO has a d_{y2}-like shape and the $2a_1$ MO extends along the *z*- axis with the larger lobe inside the Cl—Zr—Cl angle. The b_2 orbital is contributed to mainly by the d_{yz} orbital (see Fig. 3 by Lauher & Hoffmann, 1976). Experimental electron density maps in Fig. 4 give a good illustration of this statement. Indeed, negative deformation densities along the *y* axis can be associated with a manifestation of the $1a_1$ vacant non-bonding orbital of Zr. The charge concentration inside the Cl—Zr—Cl angle in the *yz* plane (Fig. 4 and Fig. 5) is related to the overlapped $2a_1$ and b_2 orbitals of the Zr atom and the p_π-orbitals of the Cl atoms. The charge-deficient region around the Zr atom along the negative *z* direction (Fig. 4*a*–*d*) may be related to the anti-bonding contribution of the d_{z^2} AO of this atom to the $2a_1$ MO.

An approximate scheme by Holladay *et al.* (1983) and Sabino & Coppens (2003), based on crystal-field theory, allows 4*d*-orbital populations of the Zr atom to be derived from the multipole parameters describing the deformation density. These populations are given in Table 5 (the tetrahedral symmetry restriction has not been applied). All the valence electrons were assumed to be described by the 4*d* electrons and the covalent contribution to all the Zr–ligand bonds was ignored. However, as demonstrated above, the Zr—C2 inter-

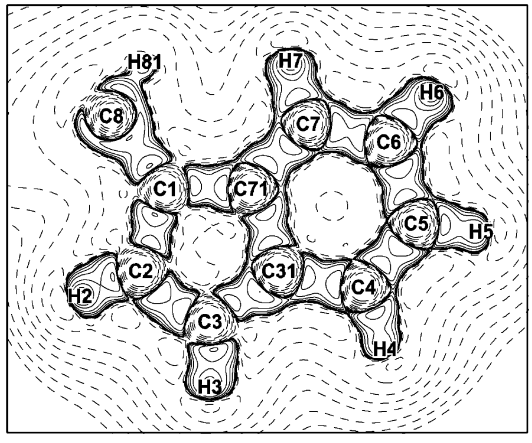

Figure 6
Laplacian of the electron density in the mean-square plane going through the indenyl ligand. The line intervals are $\pm(2, 4, 8) \times 10^n$ e Å^{-5} ($-2 \le n \le 2$), negative values are solid.

Table 6
Topological and Pauling's bond orders for C—C bonds in *rac*-EBIZD.

Bonds	Topological bond order	Pauling bond order	Bonds	Topological bond order	Pauling bond order
C1—C2	1.30	1.39	C31—C71	1.02	1.32
C1—C71	1.17	1.40	C4—C5	1.58	1.68
C1—C8	0.90	1.06	C5—C6	1.22	1.37
C2—C3	1.31	1.41	C6—C7	1.56	1.67
C3—C31	1.19	1.41	C7—C71	1.20	1.37
C31—C4	1.23	1.39	C8—C8′	0.66	0.95

action is intermediate between the closed-shell and shared interactions; that means that electrons are partially shared by the interacting atoms. In addition, some of the 5*s* electrons are probably localized within the Zr atom basin. As a result, the electron populations in Table 5 are far from the idealized values from the crystal-field theory consideration of tetrahedral symmetry.

4.5. Electron density in the indenyl ligand

The valence and deformation electron densities (Fig. 4), the Laplacian of the electron density (Fig. 6) and the C—C bond critical-point characteristics (Table 2) show the main features of the electron distribution in the conjugated indenyl system. Electron density at the bond centers is elongated perpendicular to the ring planes, reflecting the π component of the C—C bond, while the Laplacian shows a charge concentration along the C—C vector which is related to the σ-component of this bond. At the same time, all the characteristics and functions mentioned above show that the electron distributions for the indenyl ligands are affected by both the interaction with the $ZrCl_2$ moiety and the presence of the ansa-bridge.

We are now attempting to connect the electron density features in the indenyl ligands with orbital-based bond descriptors. Cioslowski & Mixon (1991) have proposed the bond-order index n_C, which combines the topological consideration and the orbital description of the bonds. They suggested that bond orders would be best computed on a localized orbital basis which maximizes the sum of the squared diagonal elements of the atomic overlap matrices. Elements of these matrices are computed by integrating the orbital products over the zero-flux atomic basins used in the topological analysis. Each bond order, n_C, is computed by summing the corresponding diatomic contributions. Howard & Lamarche (2003) have found that Cioslowski & Mixon's bond order can be well approximated by the expression $n_C = a + b\lambda_3 + c(\lambda_1 + \lambda_2) + d\rho_b$, which is suitable for both ordinary and multiple bonds (λ_i are the electron density curvatures and ρ_b is the electron density at the bond critical point). With this approximation, Cioslowski & Mixon's bond order can be directly estimated using the topological characteristics of experimentally derived electron density.

We have applied this approach to quantify the C—C bonds in the indenyl ligand (Table 6). The following coefficient values recommended by Howard & Lamarche (2003) for the C—C bonds were used: $a = -0.522$, $b = -1.695$, $c = 0$, $d = 8.473$. Pauling's (1960) widely accepted quantitative measure of bond order, $n_P = \exp[(r_0 - R)/a]$ depending only on the bond length R, was also calculated using the values $r_0 = 1.521$ and $a = 0.293$ (Howard & Lamarche, 2003). Table 6 shows that Pauling's bond order is the same for bonds of equal length (*cf. e.g.* C2—C3 and C3—C31 bonds) and that the bond order in the indenyl rings is close to the formal value of 1.5. At the same time the index n_C, which explicitly reflects the actual electron distribution, varies for C—C bonds of the same length and reveals a difference in the indenyl ring bond strengths due to the effects of ligand interaction with the environment.

We note that the index n_C shows magnitudes lower than the formal values. According to Angyan *et al.* (1994) this results from the fact that the n_C index mainly reflects the covalent part of the bond order. In spite of that, the n_C index is proved to be a suitable descriptor of the bond order and we can recommend it for use in the treatment of experimental electron densities.

In conclusion, the topological analysis of the electron density in racemic ethylenebis(1-indenyl)zirconium dichloride derived from accurate X-ray diffraction data allowed us to obtain a new insight into the electronic structure of the title compound. The metal–indenyl bonding is characterized by only one Zr—C2 bond path which is significantly curved towards the C1—C2 bond. Simultaneously, the π-electrons of the C1—C2 bond are significantly involved in the metal–ligand interaction. The electron density features point towards the conclusion that the indenyl coordination can be approximately described as η^1 with slippage towards η^2. The 'ligand-opposed' charge concentrations around the Zr atom were revealed using the distributions of the Laplacian of the electron density and the one-particle potential. This work and other similar findings (Bytheway *et al.*, 1996; Bader & Matta, 2001; Lyssenko *et al.*, 2003; Pillet *et al.*, 2003) show that the bonding picture in bent metallocenes is more complicated than is often followed from the simple classic view.

The charge transfer from the Zr atom to both indenyl ligands and the two Cl atoms has been estimated and all the atomic interactions have been quantitatively characterized in terms of the electron density and energy-density features at the bond critical points. In addition, the C—C bonds in the indenyl ligand were described using the Cioslowski–Mixon bond-order indices calculated directly from the experimental electron density. Such information is of importance for understanding the nature of bonding in the metal complexes.

The support of this work by the Japan Ministry of Education, Science, Sports and Culture (grant # 09045034) and the Russian Foundation for Basic Research (grant 04-03-33053) is gratefully acknowledged. VGT thanks Professor W. A. Herrmann and Professor M. Tamm for the hospitality during his stay at München Technical University and the Alexander von Humboldt Foundation (Germany) for a Humboldt Senior Scientist Research Prize.

References

Abramov, Yu. A. (1997). *Acta Cryst.* A**53**, 264–272.
Angyan, J., Loos, M. & Mayer, I. (1994). *J. Phys. Chem.* **98**, 5244–5248.
Antipin, M. Yu., Lyssenko, K. A. & Boese, R. (1996). *J. Organomet. Chem.* **508**, 259–262.
Bader, R. F. W. (1990). *Atoms in Molecules – A Quantum Theory.* Oxford University Press.
Bader, R. F. W. & Beddall, P. M. (1972). *J. Chem. Phys.* **56**, 3320–3329.
Bader, R. F. W., Gillespie, R. J. & Martin, F. (1998). *Chem. Phys. Lett.* **290**, 488–494.
Bader, R. F. W. & Matta, C. F. (2001). *Inorg. Chem.* **40**, 5603–5611.
Becke, A. D. & Edgecombe, K. E. (1990). *J. Chem. Phys.* **92**, 5397–5403.
Becker, P. & Coppens, P. (1974). *Acta Cryst.* A**30**, 129–147.
Belelli, P. G., Damiani, D. E. & Castellani, N. J. (2004). *J. Mol. Catal. A*, **208**, 147–158.
Bianchi, R., Gervasio, G. & Marabello, D. (2000). *Inorg. Chem.* **39**, 2360–2366.
Brintzinger, H. H., Fischer, D., Muelhaupt, R., Rieger, B. & Waymouth, R. M. (1995). *Angew. Chem. Int. Ed. Engl.* **34**, 1143–1170.
Bythway, I., Gillespie, R. G., Tang, T.-H. & Bader, R. F. W. (1995). *Inorg. Chem.* **34**, 2704–2714.
Bytheway, I., Popelier, P. L. A. & Gillespie, R. J. (1996). *Can. J. Chem.* **74**, 1059–1071.
Coppens, P., Iversen, B. & Larsen, F. K. (2005). *Coord. Chem. Rev.* **249**, 179–195.
Cioslowski, J. & Mixon, S. T. (1991). *J. Am. Chem. Soc.* **113**, 4142–4145.
Ewen, J. (1984). *J. Am. Chem. Soc.* **106**, 6355–6364.
Espinosa, E., Alkorta, I. & Elguero, J. & Molins, E. (2002). *J. Chem. Phys.* **117**, 5529–5542.
Espinosa, E., Molins, E. & Lecomte, C. (1998). *Chem. Phys. Lett.* **285**, 170–173.
Fan, M.-F. & Lin, Zh. (1998). *Organometallics*, **17**, 1092–1100.
Farrugia, L. J., Mallinson, P. R. & Stewart, B. (2003). *Acta Cryst.* B**59**, 234–247.
Frenking, G., Wichmann, K., Froehlich, N., Loschen, C., Lein, M., Frunzke, J. & Rayon, V. M. (2003). *Coord. Chem. Rev.* **238–239**, 55–82.
Gillespie, R. G., Bythway, I., Tang, T.-H. & Bader, R. F. W. (1996). *Inorg. Chem.* **35**, 3954–3563.
Gillespie, R. J., Noury, S., Pilme, J. & Silvi, B. (2004). *Inorg. Chem.* **43**, 3248–3256.
Green, J. C. (1998). *Chem. Soc. Rev.* **27**, 263–271.
Hansen, N. K. & Coppens, P. (1978). *Acta Cryst.* A**34**, 909–921.
Holladay, A., Leung, P. & Coppens, P. (1983). *Acta Cryst.* A**39**, 377–387.
Howard, S. T. & Lamarche, O. (2003). *J. Phys. Org. Chem.* **16**, 133–141.
Hunter G. (1975). *Int. J. Quant. Chem.* **9**, 237–242.
Hwang, T.-S. & Wang, Yu. (1998). *J. Phys. Chem. A*, **102**, 3726–3731.
Ivchenko, P. V. & Nifantiev, I. E. (1998). *Zh. Org. Khim.* **34**, 9–38.
Kaminsky, J. & Arndt, M. (1997). *Adv. Polym. Sci.* **127**, 143–187.
Kaminsky, J., Kuelper, K., Brintzinger, H. H. & Wild, F. (1985). *Angew. Chem. Int. Ed. Engl.* **24**, 507–508.
Kirzhnits, D. A. (1957). *Sov. Phys. JETP*, **5**, 64–72.
Kohout, M., Savin, A. & Press, H. (1991). *J. Chem. Phys.* **95**, 1928–1942.
Koritsanszky, T. & Coppens, P. (2001). *Chem. Rev.* **101**, 1583–1628.
Lauher, J. W. & Hoffmann, R. (1976). *J. Am. Chem. Soc.* **98**, 1729–1742.
Lee, H., Lee, C. & Parr, R. G. (1991). *Phys. Rev. A*, **44**, 768–771.
Lee, C.-R., Wang, C.-C., Chen, K.-C., Lee, G.-H. & Wang, Y. (1999). *J. Phys. Chem. A*, **103**, 156–165.
Linnolahti, M., Hirva, P. & Pakkanen, P. A. (2001). *J. Comput. Chem.* **22**, 51–64.
Long, N. J. (1998). *Metallocenes.* Oxford: Brackwell Science.
Lyssenko, K. A., Antipin, M. Yu. & Ketkov, S. Yu. (2001). *Russ. Chem. Bull. Int. Ed.* **50**, 130–141.
Lyssenko, K. A., Golovanov, D. G. & Antipin, M. Yu. (2003). *Mendeleev Commun.* pp. 209–211.
Macchi, P. & Coppens, P. (2001). *Acta Cryst.* A**57**, 656–662.
Macchi, P., Proserpio, D. M. & Sironi, A. (1998). *J. Am. Chem. Soc.* **120**, 13429–13435.
Macchi, P. & Sironi, A. (2003). *Coord. Chem. Rev.* **238–239**, 383–412.
Marabello, D., Bianchi, R., Gervasio, G. &. Cargnoni, F. (2004). *Acta Cryst.* A**60**, 494–501.
Martin Pendas, A., Costales, A. & Luana, V. (1997). *Phys. Rev. B*, **55**, 4275–4284.
Nesmeyanov, A. N., Volkenau, N. A. & Vilchevskaya, V. D. (1956). *Dokl. Akad. Nauk SSSR*, **111**, 362–364.
Parr, R. G. & Yang, W. (1989). *Density-Functional Theory of Atoms and Molecules.* New York: Oxford University Press.
Piemontesi, F., Camurati, I., Resconi, L., Balboni, D., Sironi, A., Moret, M., Zeigler, R. & Piccolrovazzi, N. (1995). *Organometallics*, **14**, 1256–1266.
Pillet, S., Wu, G., Kulsomphob, V., Harvey, B. G., Ernst, R. D. & Coppens, P. (2003). *J. Am. Chem. Soc.* **125**, 1937–1949.
Pauling, L. (1960). *The Nature of the Chemical Bond.* Ithaca, New York: Cornell University Press.
Popelier, P. L. A., Aicken, F. M. & O'Brien, S. E. (2000). *Specialist Periodical Report, Chemical Modeling: Applications and Theory*, edited by A. Hinchliffe, Vol. 1, pp. 143–198.. The Royal Society of Chemistry.
Protas, J. (1997). *MOLDOS*97/*MOLLY MS DOS* Updated Version. Private Communication.
Rinehart, K. L. & Curby, R. J. (1957). *J. Am. Chem. Soc.* **79**, 3290–3291.
Sabino, J. R. & Coppens, P. (2003). *Acta Cryst.* A**59**, 127–131.
Sagar, R. P., Ku, A. C. T., Smith, V. H. & Simas, A. M. (1988). *J. Chem. Phys.* **88**, 4367–4374.
Schaefer, A., Karl, E., Zsolnai, L., Huttner, G. & Brintzinger, H. H. (1987). *J. Organomet. Chem.* **328**, 87–99.
Scherer, W. & McGrady, G. S. (2004). *Angew. Chem. Int. Ed. Engl.* **43**, 1782–1806.
Schmider, H. L. & Becke, A. D. (2000). *J. Mol. Struct. (Theochem.)* **527**, 51–61.
Schmider, H., Sagar, R. P. & Smith, V. H. (1991). *J. Chem. Phys.* **94**, 8627–8629.
Sheldrick, G. M. (1997*a*). *SHELXS*97. University of Göttingen, Germany.
Sheldrick, G. M. (1997*b*). *SHELXL*97. University of Göttingen, Germany.
Shi, Z. & Boyd, R. J. (1988). *J. Chem. Phys.* **88**, 4375–4377.
Smith, G. T., Malinson, P. R., Frampton, C. S., Farrugia, L. J., Peacock, R. D. & Howard, J. A. K. (1997). *J. Am. Chem. Soc.* pp. 5028–5034.
Stash, A. I. (2003). Proc. for the 28th ISTC Japan Workshop on Frontiers of X-ray Diffraction Technologies, Russia/CIS, Nagoya, pp. 147–153.
Stash, A. I. & Tsirelson, V. G. (2002). *J. Appl. Cryst.* **35**, 371–373.
Stash, A. I. & Tsirelson, V. G. (2005). *Crystallogr. Rep.* **50**, 177–184.
Tafipolsky, M., Scherer, W., Öfele, K., Artus, G., Pedersen, B., Herrmann, W. A. & McGrady, G. S. (2002). *J. Am. Chem. Soc.* **124**, 5865–5880.
Tamm, M., Kunst, A., Bannenberg, T., Herdtweck, E., Sirsch, P., Elsevier, C. & Ernsting, J. M. (2004). *Angew. Chem. Int. Ed. Engl.* **43**, 5530–5534.
Tanaka, K. & Saito, Y. (1975). *Acta Cryst.* A**31**, 841–845.
Togni, A. (1998). Editor. *Metallocenes.* Weinheim, Germany: Wiley-VCH.
Tsirelson, V. (1999). *Acta Cryst.* A**55** Supplement, Abstract M13-OF-003.

Tsirelson, V. G. (2002). *Acta Cryst.* B**58**, 632–639.
Tsirelson, V. G. (2003). 3rd Europian Charge Density Meeting and Europian Science Foundation Exploratory Workshop (ECDM-III). Sandbjerg Estate, Denmark, 2003, p. O7.
Tsirelson, V. G. & Ozerov, R. P. (1996). *Electron Density and Bonding in Crystals.* Bristol and Philadelphia: IOP.
Tsirelson, V. & Stash, A. (2002*a*). *Chem. Phys. Lett.* **351**, 142–148.
Tsirelson, V. & Stash, A. (2002*b*). *Acta Cryst.* B**58**, 780–785.
Tsirelson, V. & Stash, A. (2004). *Acta Cryst.* A**60**, 418–426.
Wang, C.-C., Wang, Y., Liu, H.-J., Lin, K.-J., Chou, L.-K. & Chan, K-S. (1997). *J. Phys. Chem. A*, **101**, 8887–8901.
Weits, R., Rees, B., Mitschler, A. & Mathey, F. (1981). *Inorg. Chem.* **20**, 2966–2970.
Wild, F., Wasiucionek, M., Huttner, G. & Brintzinger, H. H. (1985). *J. Organomet. Chem.* **288**, 63–67.
Xu, Z.-F., Xie, Y., Feng, W.-L. & Schaeffer, H. F. (2003). *J. Phys. Chem. A*, **107**, 2716–2729.
Zachmanoglu, C. E., Docrat, A., Bridgewater, B. M., Parkin, G., Brandow, C. G., Bercaw, J. E., Jardine, C. N., Lyall, M., Green, J. C. & Keister, J. B. (2002). *J. Am. Chem. Soc.* **124**, 9525–9546.
Zou, P. F. & Bader, R. F. W. (1994). *Acta Cryst.* A**50**, 714–724.